Bulletin of the Seismological Society of America. Vol. 59, No. 4, pp. 1667–1693. August, 1969

UNIVERSAL DISPERSION TABLES

III. FREE OSCILLATION VARIATIONAL PARAMETERS

By Don L. Anderson and Robert L. Kovach

ABSTRACT

The effect of a small change in any parameter of a realistic Earth model on the periods of free oscillation is computed for both spheroidal and torsional modes. The normalized partial derivatives, or variational parameters, are given as a function of order number and depth in the Earth. For a given mode it can immediately be seen which parameters and which regions of the Earth are controlling the period of free oscillation. Except for ${}_0S_0$ and its overtones the low-order free oscillations are relatively insensitive to properties of the core. The shear velocity of the mantle is the dominant parameter controlling the periods of free oscillation and density can be determined from free oscillation data only if the shear velocity is known very accurately. Once the velocity structure is well known free oscillation data can be used to modify the average density of the upper mantle. The mass and moment of inertia are then the main constraints on how the mass must be redistributed in the lower mantle and core.

Introduction

Free oscillation data provide constraints on the elastic properties and density of the Earth that supplement body wave velocity data, mass and moment of inertia. However, the calculation of the periods of free oscillation of a realistic Earth model is a tedious and time consuming chore, even on a large electronic computer. Because of the large number of parameters involved it is difficult to modify a standard or trial Earth model to obtain agreement with free oscillation observations. The partial derivatives given in this paper allow one to determine which parameters are most important for any given mode and which parameters have little influence. In particular, they allow one to assess the effect of density, the main parameter which has been modified on the basis of free oscillation data. Comparison of the partial derivatives for various modes also allows one to assess the independence or lack thereof of these modes and therefore the degree of redundance of the information contained in a given set of modes.

In addition to the qualitative use of the perturbation parameters, discussed above, they can also be used, in a matrix inversion scheme, to modify, to first order, the trial structure in order to fit a given set of observed free oscillation data.

List of Symbols Used

a, radius of earth
α, compressional wave velocity
β, shear wave velocity
g, gravitational acceleration
G, gravitational constant
l, integer denoting surface harmonic dependence on polar angle
λ, Lame constant
μ, rigidity
n, number of radial nodal surfaces

$P(r)$, radial factor in the perturbation of the gravitational potential
ρ, density
${}_nU_l(r)$, radial function in the vertical component of displacement for spheroidal oscillations
${}_nV_l(r)$, radial function in horizontal component of displacement
${}_nW_l(r)$, radial function in the torsional oscillations
ω, angular frequency

Theory

We use the variational method, first used in a geophysical context by Stoneley (1926) and Jeffreys (1935) and applied by Anderson (1964), Anderson and Harkrider (1968). Archambeau and Anderson (1964), Takeuchi et al. (1964) and Wiggins (1968). The variational parameters or partial derivatives, can be expressed in terms of ratios of energy integrals as discussed in Archambeau and Anderson (1964). Most of the appropriate theory is summarized in Backus and Gilbert (1967). For brevity we shall only illustrate how the variational parameters are derived for the torsional oscillations.

For the torsional oscillations the kinetic and potential energies averaged over a cycle are, apart from constant factors,

$$T = \omega^2 \int_0^r \rho(r) W_l^2(r) r^2 \, dr$$

$$V = \int_0^r \mu(r) \{ \dot{W}_l^2(r) r^2 - 2\dot{W}_l W_l r - W_l^2 + l(l+1) W_l^2 \} \, dr$$

Since the kinetic and potential energies averaged over a cycle are equal

$$\omega^2 I_0 = I_1 + l(l+1) I_2 \tag{1}$$

where

$$I_0 = \int_0^r \rho(r) W_l^2 r^2 \, dr$$

$$I_1 = \int_0^r \mu(r) \{ -W_l^2 - 2W_l \dot{W}_l r + \dot{W}_l^2 r^2 \} \, dr$$

$$I_2 = \int_0^r \mu(r) W_l^2 \, dr$$

If we vary ρ and μ retaining the same value of $W_l(r)$ we find that

$$(\omega + \delta\omega)^2 (I_0 + \delta I_0) = I_1 + \delta I_1 + l(l+1)(I_2 + \delta I_2) + \mathcal{O}[(\delta\rho)^2, (\delta\mu)^2]. \tag{2}$$

On subtracting (1) from (2) we obtain with a error of the second order

$$\delta I_0 \omega^2 + 2 I_0 \omega \delta\omega = \delta I_1 + l(l+1) \delta I_2$$

We are interested in examining the variation in the eigen-frequency $\delta\omega$ with the perturbation of a specific elastic parameter with all of the other parameters held fixed. Therefore, if we perturb the density over an interval $r - \epsilon \leqq r \leqq r + \epsilon$ holding the rigidity and the wave number k fixed we find that the change in phase velocity δc rela-

tive to the unperturbed phase velocity c is

$$\left(\frac{\delta c}{\delta \rho}\right) = - c \int_{r-\varepsilon}^{r+\varepsilon} r^2 W_l^2 \, dr/2I_0$$

or

$$\frac{\rho_i}{c}\left(\frac{\delta c}{\delta \rho}\right)_\mu = - \int_{r-\varepsilon}^{r+\varepsilon} \rho_i r^2 W_l^2 \, dr/2I_0 \tag{3}$$

which we immediately recognize as the ratio of the kinetic energy over the interval which is perturbed divided by the total energy in the system. In a similar manner we can show that

$$\frac{\mu_i}{c}\left(\frac{\delta c}{\delta \mu}\right)_\rho = \int_{r-\varepsilon}^{r+\varepsilon} \mu_i \{-W_l^2 - 2W_l \dot{W}_l r + r^2 \dot{W}_l^2 + l(l+1) W_l^2\} \, dr/2\omega^2 I_0$$

recognizable as the potential energy of the perturbed interval divided by the total energy.

For the spheroidal oscillations we can show that

$$\begin{aligned}\frac{\delta\omega}{\omega} = &- \int \delta\rho (U^2 r^2 + l(l+1) V^2 r^2) \, dr/2[I_1 + l(l+1) I_2] \\ &+ \int \delta\rho \Big\{ 8\pi G \rho U^2 r^2 - g(4U^2 r - 2l(l+1) UVr) \\ &- 8\pi G r^2 \int_r^a \rho (2U^2 r^{-1} - l(l+1) UV r^{-1}) \, dr \\ &- 2U\dot{P} r^2 - 2rl(l+1) VP \Big\} \, dr/2\omega^2 [I_1 + l(l+1) I_2]\end{aligned} \tag{5}$$

where

$$I_1 = \int_0^a \rho(r) U_l^2 r^2 \, dr$$

$$I_2 = \int_0^a \rho(r) V_l^2 r^2 \, dr.$$

If we neglect self-gravitation the second integral term in (5) can be neglected. Kovach and Anderson have shown that the gravitational energy can be neglected for $l > 7$.

Similarly

$$\begin{aligned}\frac{\lambda_i}{c}\left(\frac{\delta c}{\delta \lambda}\right)_{\mu,\rho} = &\int_{r-\varepsilon}^{r+\varepsilon} \lambda_i \{(r\dot{U}_l + 2U_l)^2 - 2l(l+1)(\dot{U}_l + 2U_l) V_l \\ &+ [l(l+1) V_l]^2\} \, dr/2\omega^2 (I_1 + l(l+1) I_2)\end{aligned}$$

$$\begin{aligned}\frac{\mu_i}{c}\left(\frac{\delta c}{\delta \mu}\right)_{\lambda,\rho} = &\int_{r-\varepsilon}^{r+\varepsilon} \mu_i \{2(r^2 \dot{U}_l^2 + 2U_l^2) + l(l+1)(U_l^2 - V_l^2 - 6U_l V_l \\ &+ 2rU_l \dot{V}_l - 2rV_l \dot{V}_l + r^2 \dot{V}_l^2) + 2[l(l+1) V_l]^2\} \, dr/2\omega^2 (I_1 + l(l+1) I_2).\end{aligned}$$

We are most concerned with the partial derivatives having α, β and ρ as independent variables. In this case

$$\left(\frac{\delta c}{\delta \beta}\right)_{\alpha,\rho} = 2\rho\beta\left\{\left(\frac{\delta c}{\delta \mu}\right)_{\lambda,\rho} - 2\left(\frac{\delta c}{\delta \lambda}\right)_{\rho,\mu}\right\}$$

$$\left(\frac{\delta c}{\delta \rho}\right)_{\alpha,\beta} = \left(\frac{\delta c}{\delta \rho}\right)_{\lambda,\mu} + (\alpha^2 - 2\beta^2)\left(\frac{\delta c}{\delta \lambda}\right)_{\rho,\mu} + \beta^2\left(\frac{\delta c}{\delta \mu}\right)_{\rho,\lambda}$$

$$\left(\frac{\delta c}{\delta \alpha}\right)_{\beta,\rho} = 2\alpha\rho\left(\frac{\delta c}{\delta \lambda}\right)_{\rho,\mu}.$$

For free oscillation studies it is convenient to have normalized partial derivatives for a change in period

$$\left(\frac{\alpha \partial T}{T \partial \alpha}\right) = \frac{-(l + \tfrac{1}{2})\alpha}{\omega a} \cdot \frac{\delta c}{\delta \alpha}$$

$$\left(\frac{\beta \partial T}{T \partial \beta}\right) = \frac{-(l + \tfrac{1}{2})\beta}{\omega a} \cdot \frac{\delta c}{\delta \beta}$$

$$\left(\frac{\rho \partial T}{T \partial \rho}\right) = \frac{-(l + \tfrac{1}{2})\rho}{\omega a} \cdot \frac{\delta c}{\delta \rho}.$$

Thus, $(\beta \partial T/T \partial \beta)_{\alpha,\rho}$ refers to the relative change in period for a relative change in shear velocity with density and compressional velocity fixed in a one kilometer thick shell at the indicated depth. We shall use normalized partial derivatives in the discussion that follows.

Standard Earth Model

The Earth model used for the present calculations evolved from the CIT11 series (Anderson and Toksöz, 1963) based on studies of long-period surface waves. It has a low-velocity zone in the upper mantle together with two major discontinuities. The compressional velocity for the mantle has been adopted from Johnson (1967). The compressional velocity in the core is modified from Gutenberg (1957), Jeffreys (1939) and Adams and Randall (1964). The shear velocity and density are functionally related to the compressional velocity and resulted from several iterations from an original trial model to reduce the residuals for the low-order modes. The model, F7M′, is shown in Figure 1 and Table 1. The computed periods for the low-order modes for model F7M′ are given in Table 2. These periods are compared with the free oscillation data in Figure 2.

The earth model has been split into 18 regions, indicated by the dashed lines in Figure 1 for the purpose of condensing the partial derivatives which are tabulated for each region. Most of the region boundaries are at natural boundaries in the Earth but a few extra regions have been inserted for additional flexibility. The partial derivatives are plotted as relative change in a period due to a relative change in the parameter in order that a whole region can be perturbed at a time.

Partial Derivatives Versus Order Number

Figures 3, 4 and 5 show the normalized partial derivatives for the fundamental spheroidal modes given as a function of order number and depth in the earth. With

TABLE 1

PARAMETERS OF MODEL F7M′

Depth (km)	V_P (km/sec)	V_S (km/sec)	ρ (g/cm^3)
0	6.14	3.70	2.83
7	6.14	3.70	2.83
25	8.12	4.75	3.32
48	8.12	4.75	3.32
65	8.01	4.56	3.22
85	8.01	4.56	3.22
95	7.93	4.38	3.25
110	7.68	4.20	3.18
130	7.50	4.20	3.09
150	7.58	4.20	3.13
170	7.70	4.33	3.15
190	8.02	4.45	3.26
210	8.32	4.45	3.42
230	8.35	4.45	3.43
250	8.40	4.45	3.46
350	8.64	4.45	3.57
365	8.70	4.45	3.60
375	8.76	4.48	3.62
385	8.79	4.55	3.79
395	8.93	4.64	3.88
405	9.21	4.86	3.99
415	9.41	5.07	3.99
430	9.51	5.17	3.93
450	9.60	5.29	3.95
470	9.66	5.36	3.97
490	9.70	5.36	3.99
600	9.93	5.36	4.11
610	9.98	5.36	4.13
630	10.13	5.41	4.19
650	10.42	5.56	4.28
690	10.86	5.92	4.38
745	11.02	6.18	4.36
800	11.09	6.26	4.35
850	11.19	6.27	4.38
900	11.27	6.29	4.41
950	11.35	6.31	4.45
1000	11.44	6.35	4.49
1200	11.77	6.48	4.62
1400	12.06	6.62	4.72
1600	12.32	6.74	4.86
1800	12.56	6.84	4.97
2000	12.77	6.94	5.06
2200	12.97	7.02	5.15
2400	13.19	7.11	5.24
2600	13.45	7.20	5.37
2700	13.58	7.24	5.38
2750	13.64	7.25	5.40
2775	13.66	6.93	5.41
2800	13.67	6.93	5.42
2844	13.69	6.93	5.44
2888	13.68	6.89	5.45
2910	8.10	0	9.90
3000	8.21	0	10.03
3202	8.48	0	10.34

TABLE 1.—*Continued*

Depth (km)	V_p (km/sec)	V_s (km/sec)	ρ (g/cm^3)
3400	8.76	0	10.67
3602	9.04	0	10.99
3800	9.29	0	11.27
4002	9.49	0	11.49
4510	10.02	0	12.10
5000	10.12	0	12.21
5044	10.11	0	12.28
5069	10.39	0	12.37
5204	11.13	0	12.62
5417	11.17	0	12.66
5892	11.23	0	12.72
6130	11.24	0	12.73
6230	11.24	0	12.73
6371	11.24	0	12.73

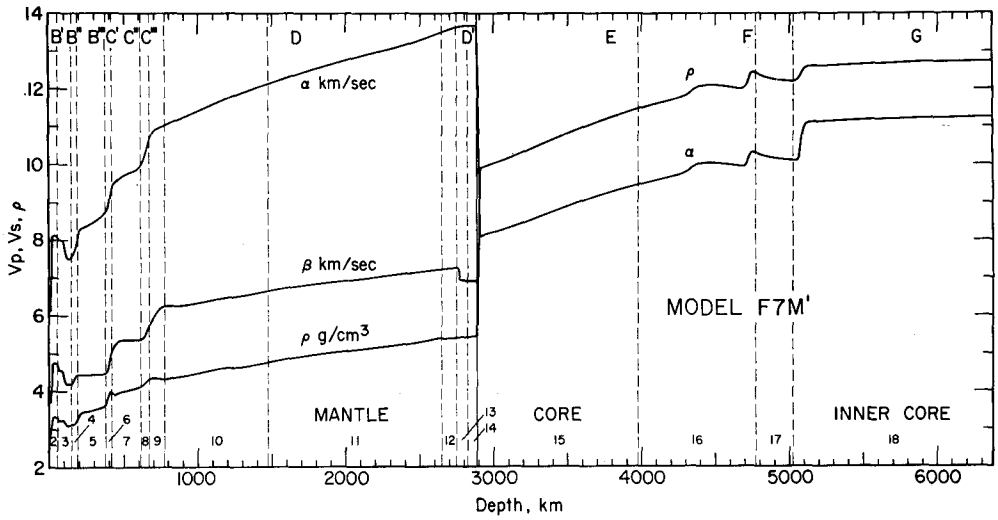

FIG. 1. Standard model F7M′ for which the variational parameters are given in this paper. The vertical dashed lines indicate the regions for which tabular values of the variational parameters are given.

this earth model the effect of increasing either the compressional and shear velocity is to decrease the period of the free oscillation. However, an increase in density can cause an increase or decrease in the p riod depending on the depth of the perturbed region and the order number (Figure 5).

The low order spheroidal modes are most sensitive to the shear velocity in the lower mantle; see, for example, the curve for 2500 km in Figure 4. Comparison of this curve with the equivalent depth curve in Figure 3 demonstrates that the compressional velocity, particularly in the lower mantle and core has little effect on the low order ($l < 8$) spheroidal modes and thus cannot be confidently extracted from free oscillation data.

The compressional velocity in the upper 500 km of the mantle has a larger effect on the low-order modes than the shear velocity and density in this region. For order numbers $l > 8$ the density becomes relatively more important. It can also be immedi-

ately seen that the low-order fundamental mode free oscillations are not particularly sensitive to density variations in the core.

Figures 6 and 7 show the partial derivatives versus order number for the torsional oscillations. The shear velocity distribution in the upper 1000 km or so is the dominant

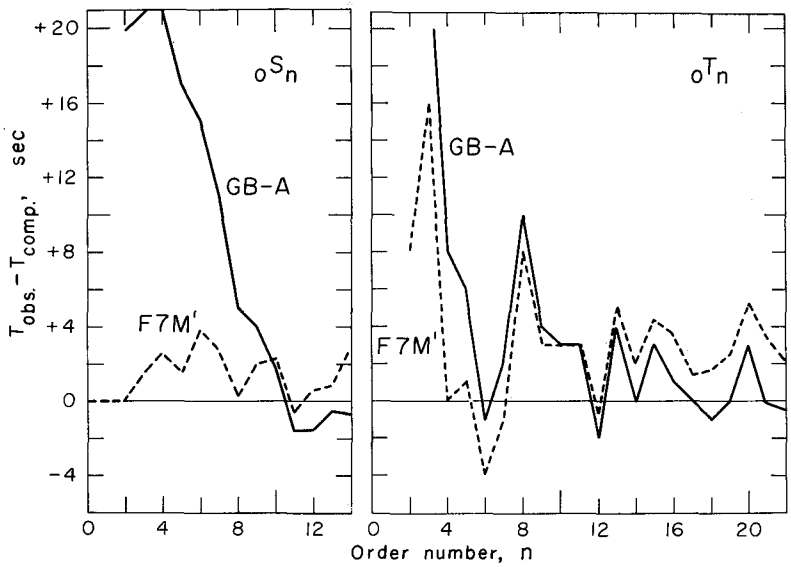

FIG. 2. Residuals for spheroidal, ${}_0S_n$, and torsional, ${}_0T_n$, modes for the Gutenberg-Bullen A model (GB-A) and F7M'.

TABLE 2

CALCULATED PERIODS OF FREE OSCILLATION (MINUTES) MODEL F7M'

Mode	T(min)	Mode	T(min)
${}_0S_0$	20.442	${}_0T_2$	43.824
${}_1S_0$	10.108	${}_0T_3$	28.350
${}_0S_2$	53.705	${}_0T_4$	21.700
${}_1S_2$	27.454	${}_0T_5$	17.894
${}_2S_2$	15.301	${}_0T_6$	15.392
${}_0S_3$	35.518	${}_0T_7$	13.598
${}_1S_3$	17.701	${}_0T_8$	12.236
${}_2S_3$	13.418	${}_0T_9$	11.158
${}_0S_4$	25.725	${}_0T_{10}$	10.279
${}_1S_4$	14.184	${}_0T_{11}$	9.545
${}_0S_5$	19.805	${}_0T_{12}$	8.921
${}_0S_6$	16.031	${}_0T_{13}$	8.382
${}_0S_7$	13.513	${}_0T_{14}$	7.911
${}_0S_8$	11.777	${}_0T_{15}$	7.495
${}_0S_9$	10.550	${}_0T_{16}$	7.124
${}_0S_{10}$	9.645	${}_0T_{17}$	6.791
${}_0S_{11}$	8.940	${}_0T_{18}$	6.490
${}_0S_{12}$	8.362	${}_0T_{19}$	6.216
${}_0S_{13}$	7.873	${}_0T_{20}$	5.966
${}_0S_{14}$	7.439	${}_0T_{21}$	5.736
${}_0S_{20}$	5.738	${}_0T_{22}$	5.524
${}_0S_{35}$	3.851	${}_0T_{25}$	4.975

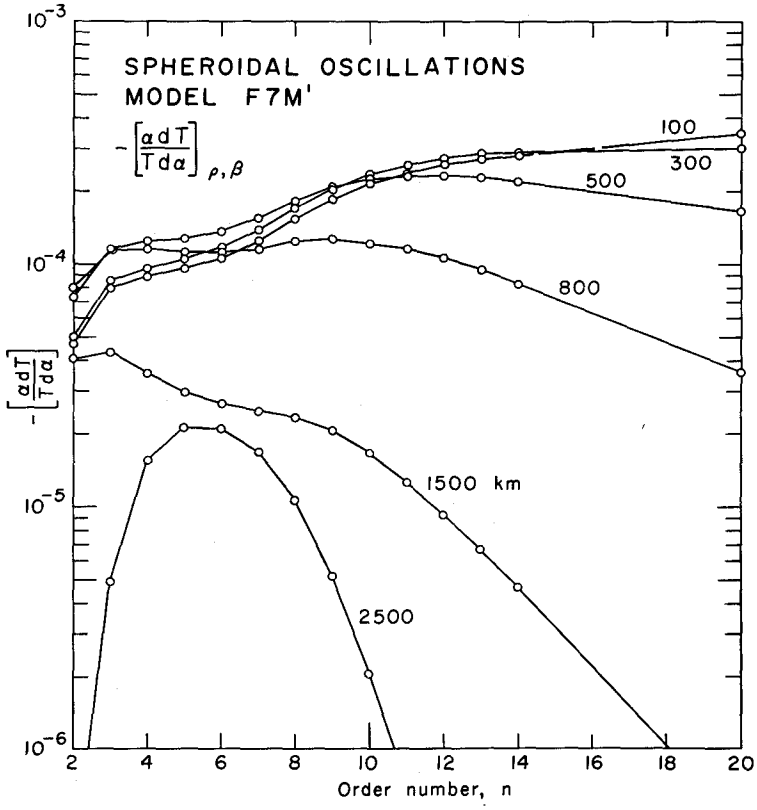

FIG. 3. Compressional velocity variational parameters as function of order number and depth for fundamental spheroidal modes.

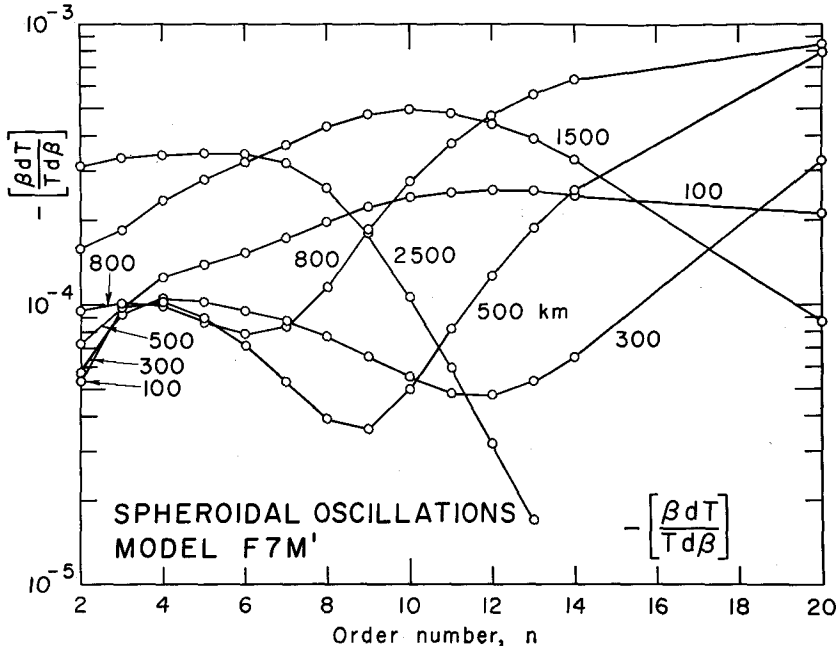

FIG. 4. Shear velocity variational parameters for fundamental spheroidal modes.

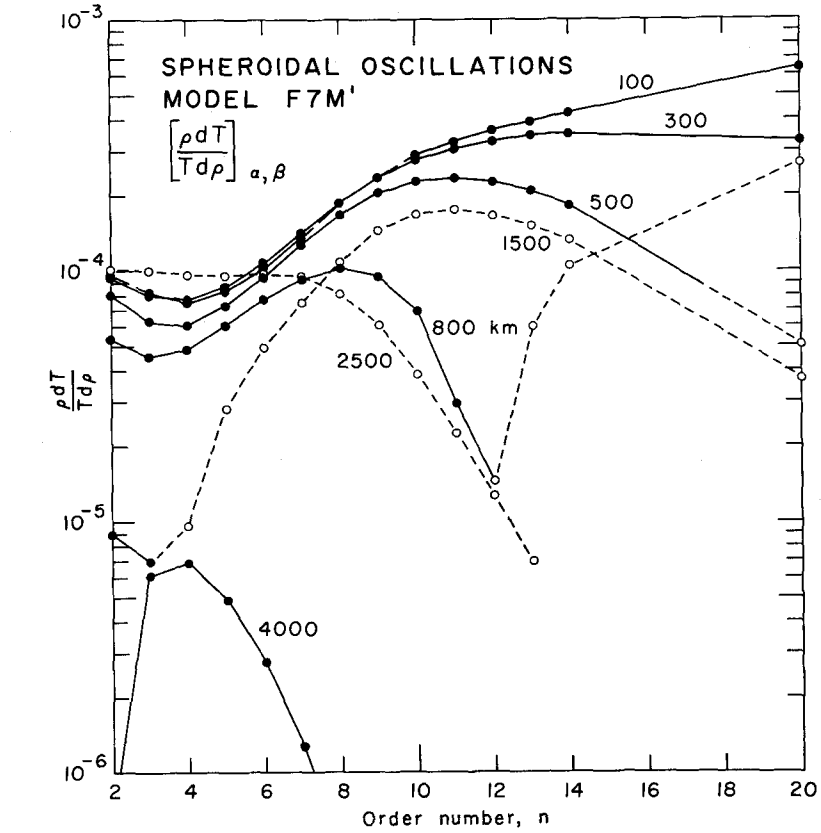

FIG. 5. Density variational parameters for fundamental spheroidal modes. Dashed lines and open circles are negative values.

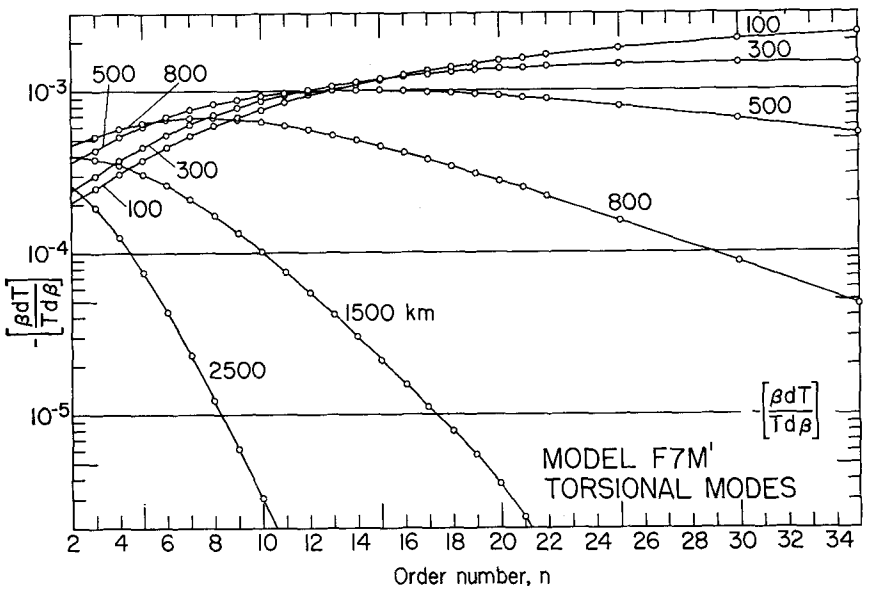

FIG. 6. Shear velocity variational parameters for fundamental torsional modes.

controlling factor for the torsional oscillations for $l < 8$. For order numbers $l > 16$ the shear velocity in the upper 400 km of the mantle controls the peroid of free oscillation.

Note that the sign of the density partial derivative can be positive or negative as was the case with the spheroidal oscillations. Figure 7 indicates that only the low-order torsional modes should be used in modifying the density distribution in the earth and that only the density of the upper 300 km of the mantle should be modified using this kind of data.

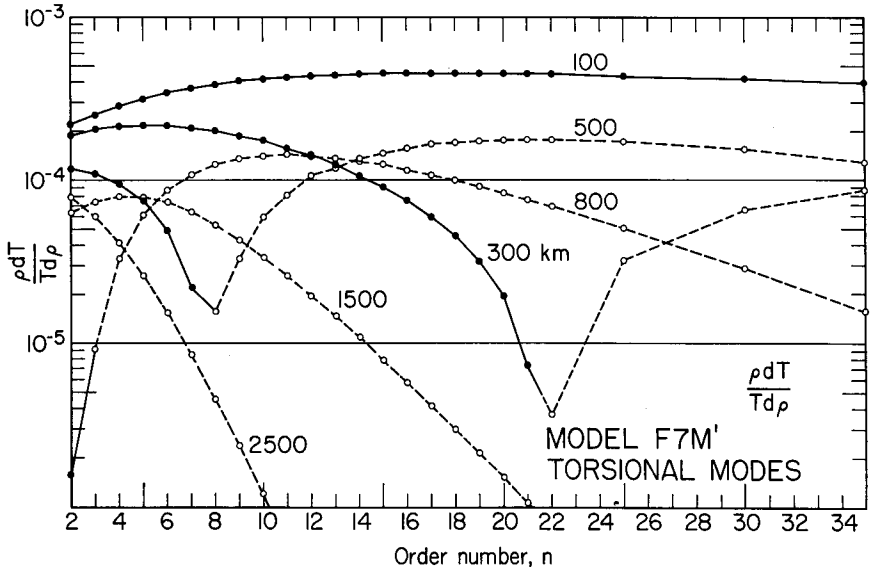

FIG. 7. Density variational parameters for fundamental torsional modes. Dashed lines and open circles are negative values.

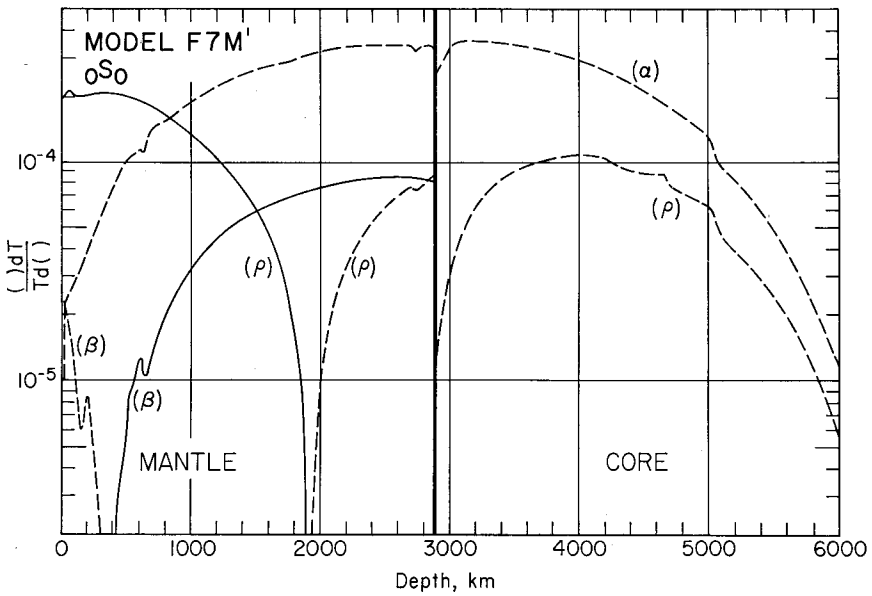

FIG. 8. Variational parameters as a function of depth for ${}_0S_0$. Dashed curves in this and the following figures refer to negative values. The values refer to a one kilometer thick layer. The fine structure is due to the normalization and reflects the structure of the Earth model.

The inverse problem in free oscillation studies is simply a matter of finding weighted linear combinations of curves such as those in Figures 3 through 7 which add up to the observed discrepancy between the observed and computed periods of free oscil-

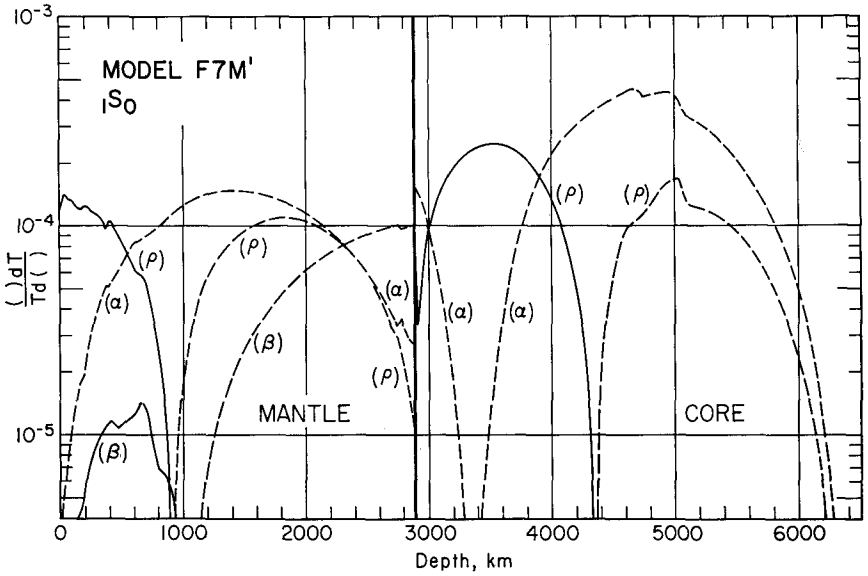

FIG. 9. Variational parameters as a function of depth for $_1S_0$.

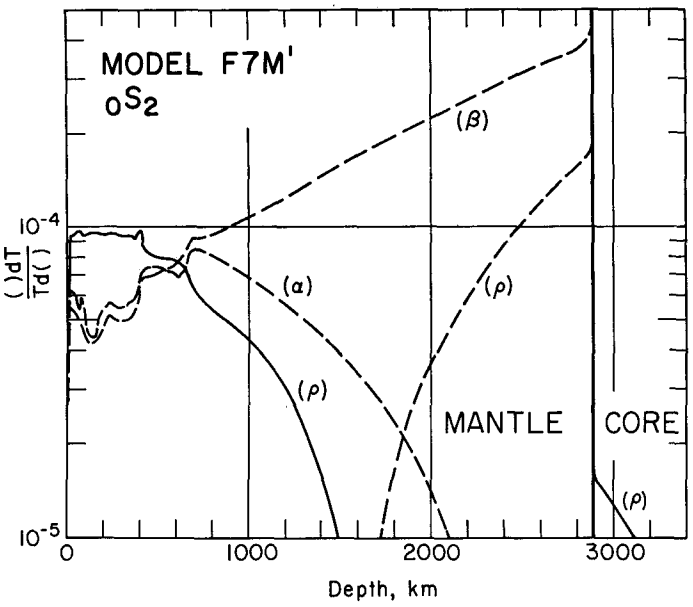

FIG. 10. Variational parameters for $_0S_2$ as a function of depth.

lation. The weighting factors are merely the relative changes in perturbation parameters which are required to make the trial model have, to first order, the observed spectrum.

PARTIAL DERIVATIVES VERSUS DEPTH

It is particularly informative to plot the normalized partial derivatives as a function of depth in the earth because this method of display makes it immediately apparent

how various parameters and regions of the Earth are being sampled by a given mode. Figure 8 shows the partial derivatives for the fundamental radial mode ${}_0S_0$. This mode is particularly insensitive to the shear velocity distribution and is primarily sensitive to the compressional velocity in the lower mantle and outer core and the density distribution in the upper mantle. Obviously if the compressional velocity distribution

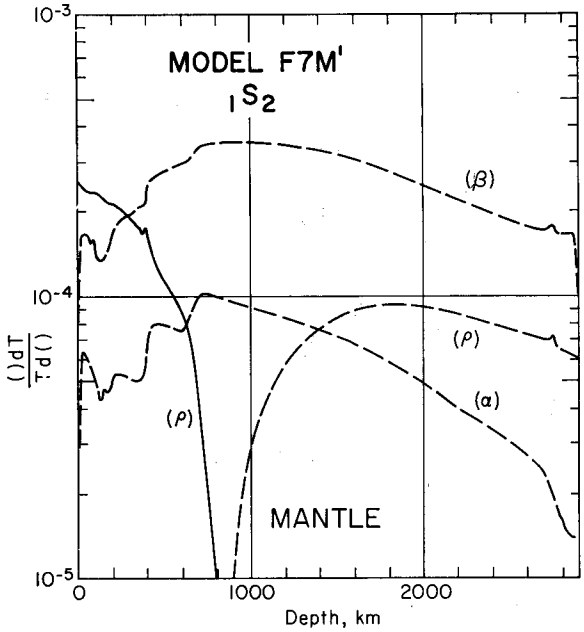

FIG. 11. Variational parameters for ${}_1S_2$ as a function of depth.

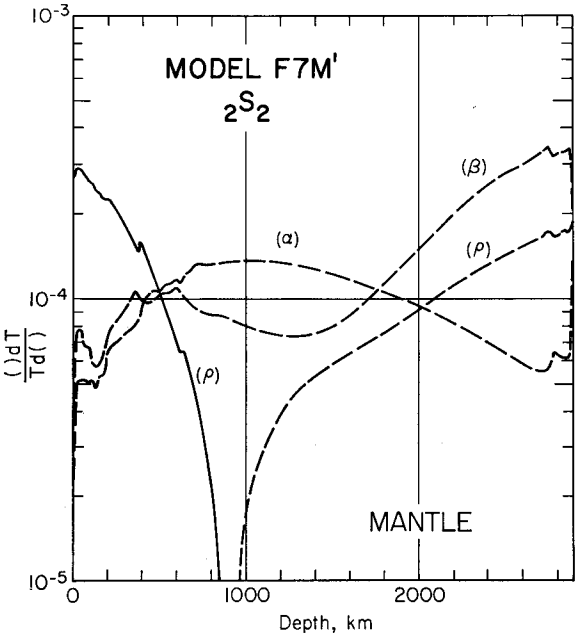

FIG. 12. Variational parameters for ${}_2S_2$ as a function of depth.

in the outer core is accurately known this mode can supply information about the density in this region. The normalized compressional velocity partial derivative is

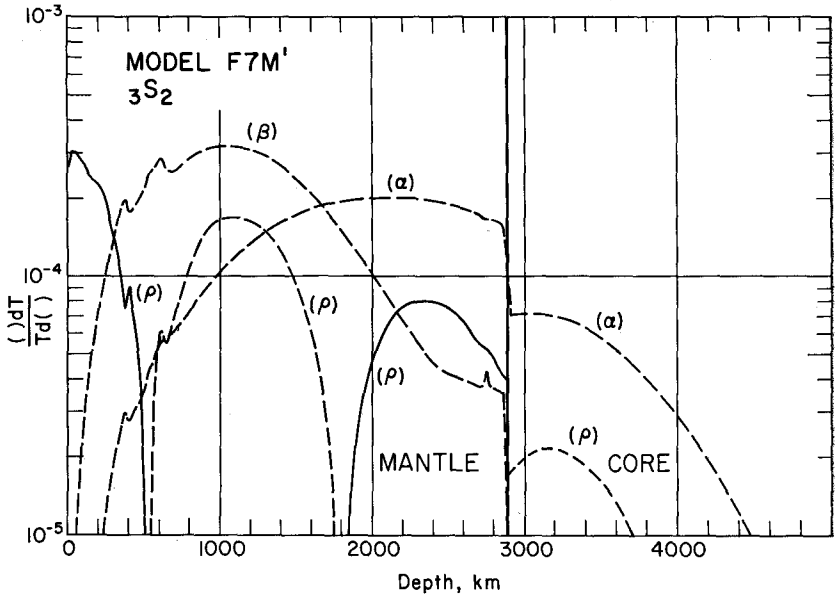

FIG. 13. Variational parameters for $_3S_2$ as a function of depth.

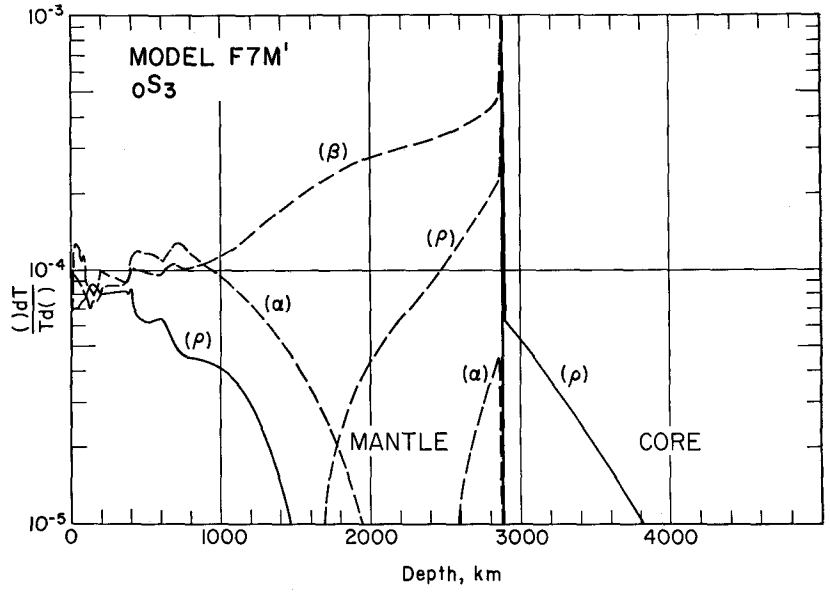

FIG. 14. Variational parameters for $_0S_3$ as a function of depth.

remarkably symmetric about the core-mantle boundary. The density partial derivative for this mode becomes negative in the lower mantle demonstrating that an increase in density in the lower mantle and core will cause a decrease in the period whereas an increase in density in the upper mantle will lengthen the period.

The behavior of the first overtone $_1S_0$ is shown in Figure 9. This mode emphasizes

structure much deeper than the fundamental mode, being particularly sensitive to the compressional velocity near the top of the outer core and the region near the top of the

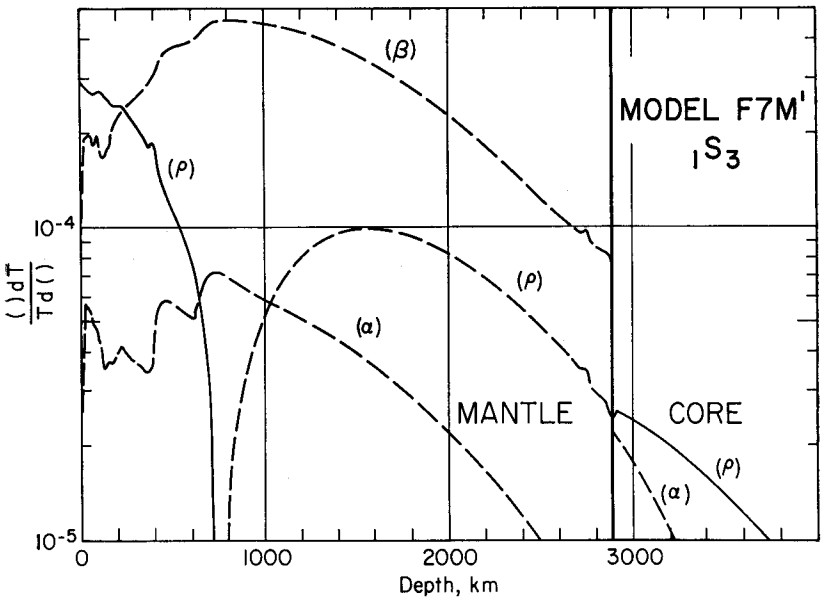

FIG. 15. Variational parameters for $_1S_3$ as a function of depth.

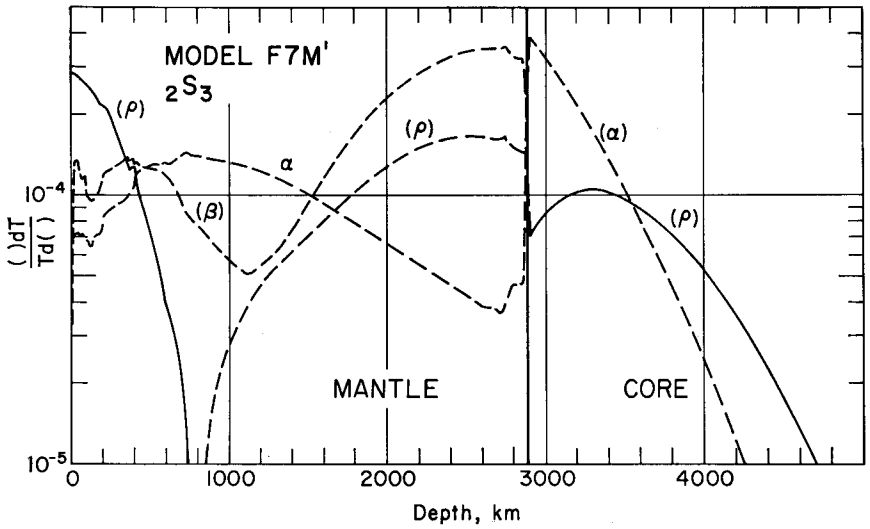

FIG. 16. Variational parameters for $_2S_3$ as a function of depth.

inner core. This mode is also sensitive to the density in the outer core and only slightly less influenced by the density in the inner core. This mode may prove useful for delineating density bounds for the inner core. The compressional velocity of the central mantle has some control on this mode but again the shear velocity is relatively unimportant in this region.

The gravest spheroidal mode $_0S_2$ samples the earth quite differently, as shown in

Figure 10. It is primarily governed by the distribution of shear velocity in the lower mantle and to a lesser extent the density in the upper 400 km of the mantle. Notice

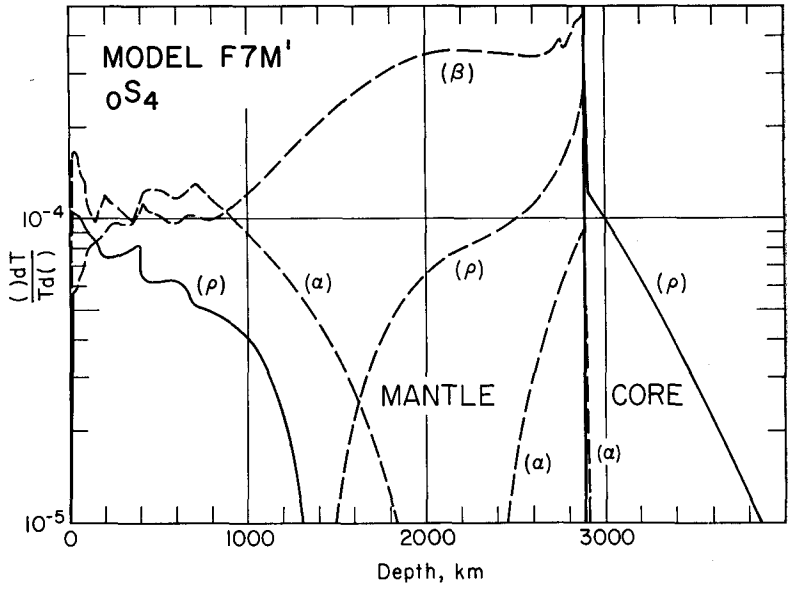

FIG. 17. Variational parameters for $_0S_4$ as a function of depth.

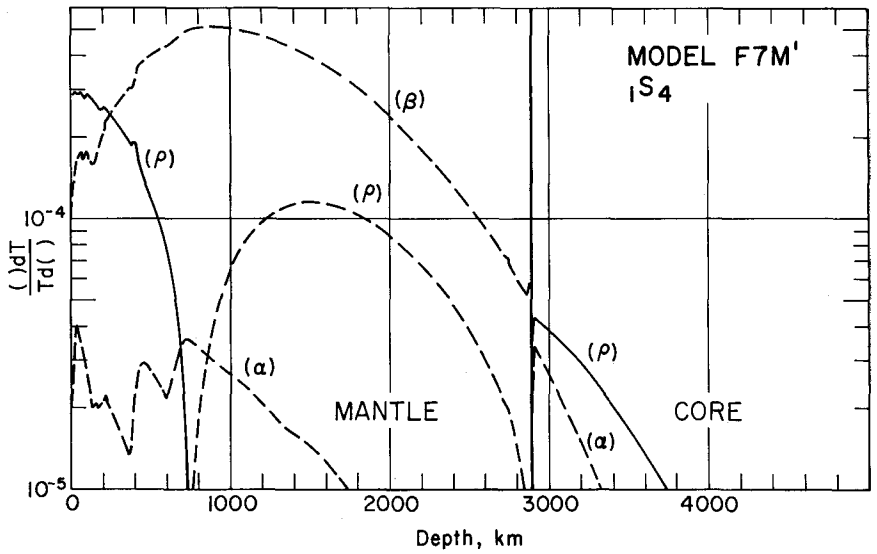

FIG. 18. Variational parameters for $_1S_4$ as a function of depth.

that the compressional velocity throughout the mantle and the velocity and density within the core have little effect on this mode. If the shear velocity in the lower mantle is accurately known then this mode can be used to refine estimates of the average density in the upper 600 km of the mantle.

The density distribution in the upper mantle becomes more important in the overtones $_1S_2$ and $_2S_2$ (Figures 11 and 12). The mode $_1S_2$ is most influenced by the shear

velocity in the central mantle, the density and compressional velocity being relatively unimportant. For ${}_2S_2$ the shear velocity in the lower mantle and the density in the

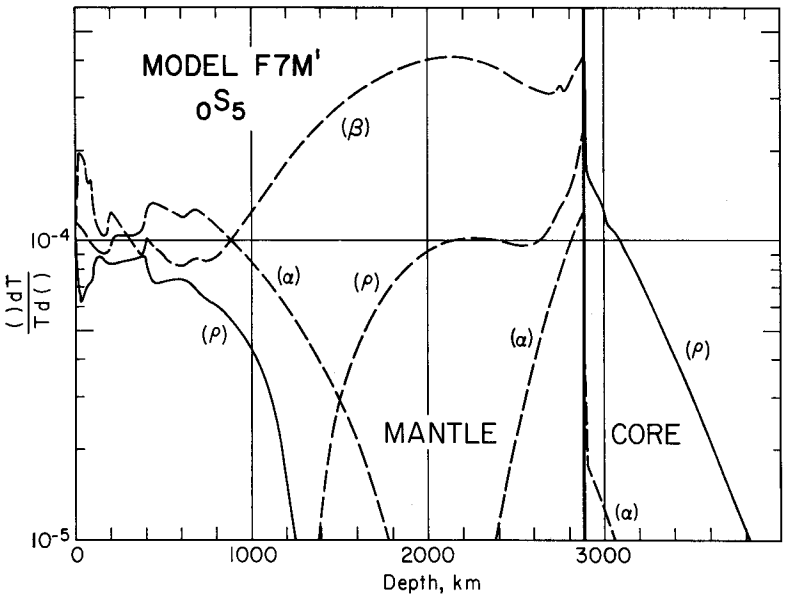

FIG. 19. Variational parameters for ${}_0S_5$ as a function of depth.

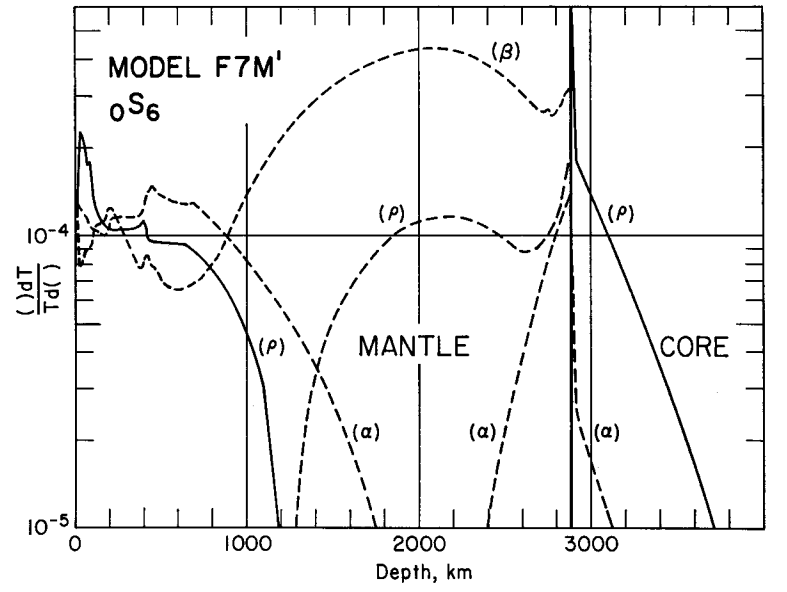

FIG. 20. Variational parameters for ${}_0S_6$ as a function of depth.

upper mantle become the controlling parameters. In the central mantle the compressional velocity dominates the other two parameters.

Figure 13 shows that the depth variation for the partial derivatives becomes increasingly complex for the higher overtones, as shown by the behavior of the mode ${}_3S_2$

in Figure 14. This mode is controlled by the shear velocity in the central mantle, the density in the upper 200 km of the mantle and to a lesser extent the compressional velocity in the lower mantle. The effect of the core is also small.

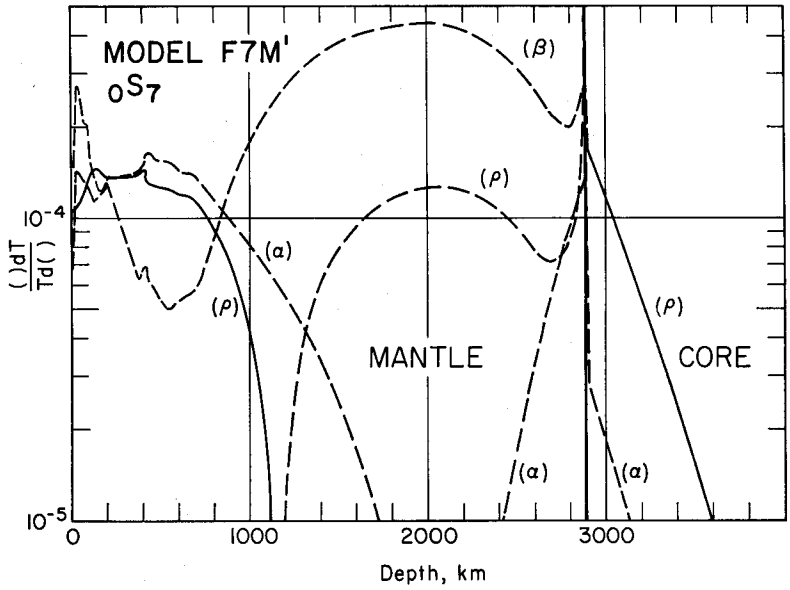

FIG. 21. Variational parameters for $_0S_7$ as a function of depth.

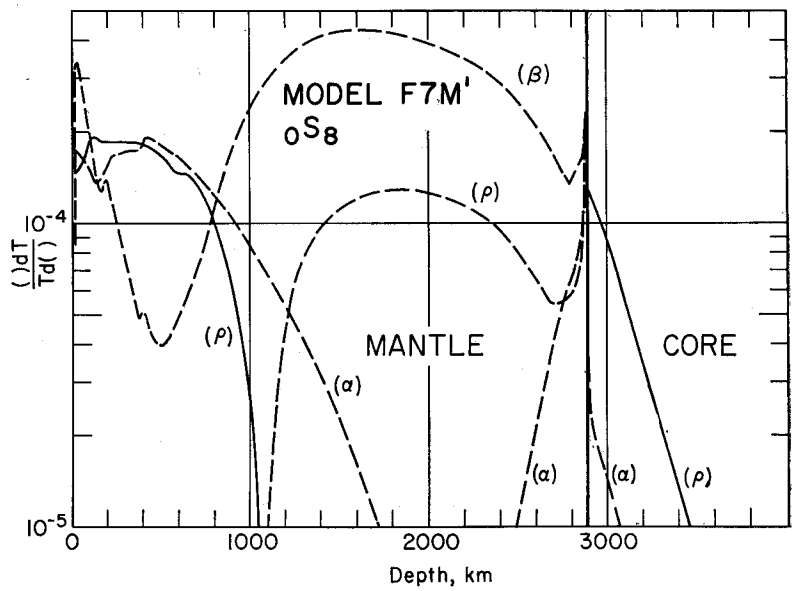

FIG. 22. Variational parameters for $_0S_8$ as a function of depth.

The modes $_0S_3$, $_1S_3$ and $_2S_3$ (Figures 14, 15 and 16) are similar to their S_2 counterparts in the manner that they sample the earth.

Modes $_0S_4$, $_1S_4$, $_0S_5$ and $_0S_6$ (Figures 17, 18, 19 and 20) are similar to their counterparts and need no further discussion. Modes $_0S_7$ through $_0S_{10}$ (Figures 21–24) point out

the increasing importance of the upper part of the lower mantle from 1000 to 2000 km depth. The strong minimum in the shear velocity perturbations between 200 and 800

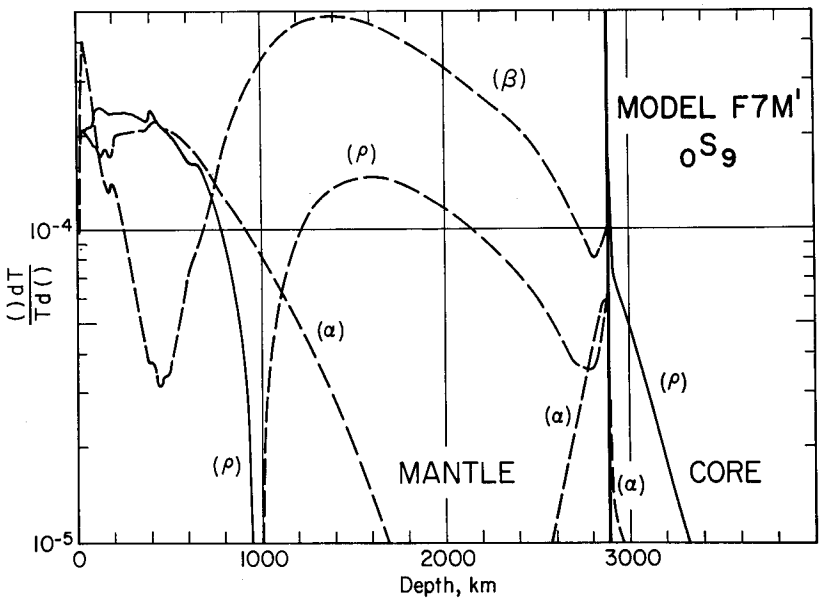

FIG. 23. Variational parameters for $_0S_9$ as a function of depth.

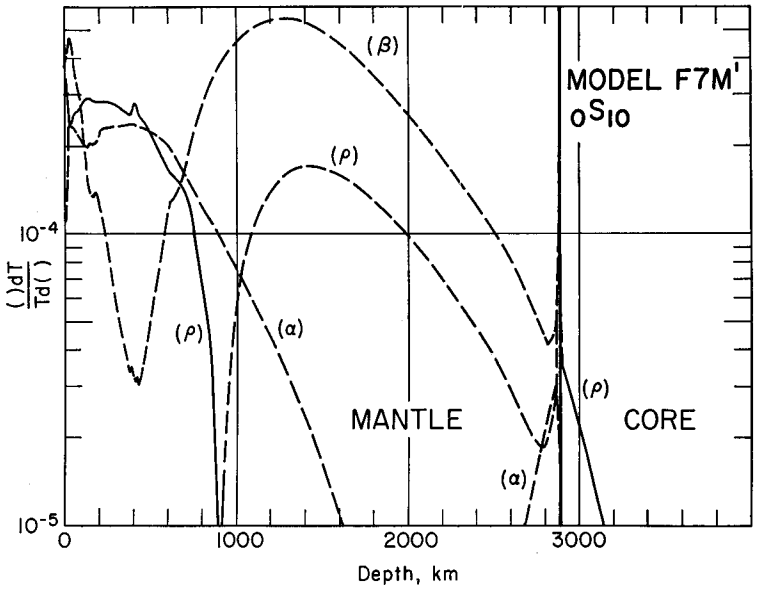

FIG. 24. Variational parameters for $_0S_{10}$ as a function of depth.

km depth shows that these modes contain little information about the shear velocity in this interesting region. On the other hand, the shear velocity partial derivatives strongly peak in the upper 100 km. The effect of changes in density and compressional velocity are comparable in the 200 to 800 km depth range.

$_0S_{13}$ (Figure 25) is strongly dominated by the shear velocity between 800 and 1400

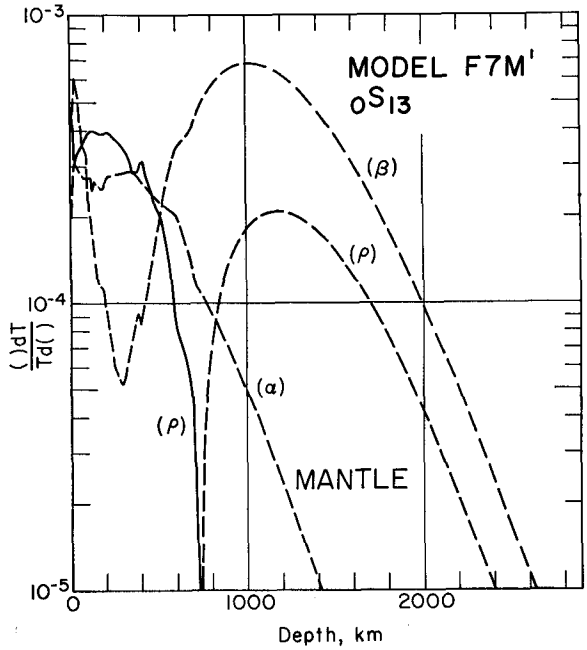

FIG. 25. Variational parameters for $_0S_{13}$ as a function of depth.

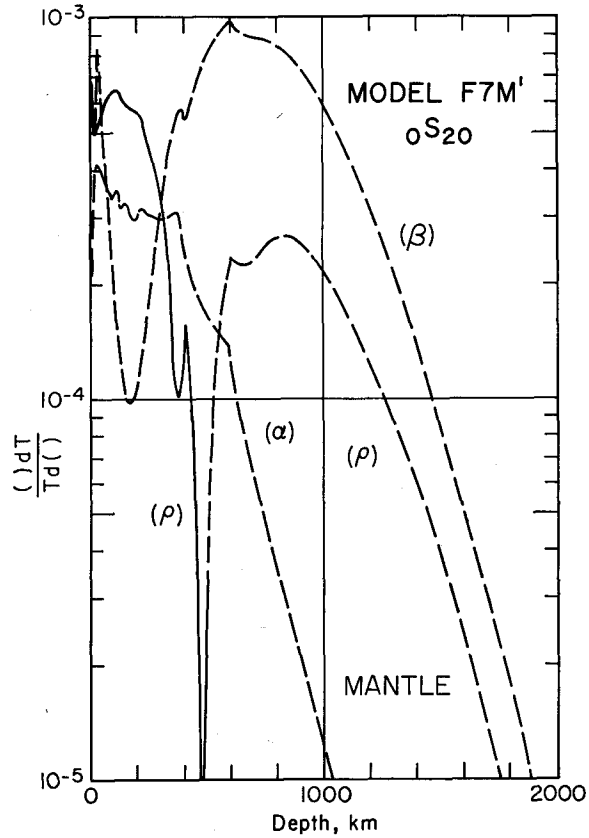

FIG. 26. Variational parameters for $_0S_{20}$ as a function of depth.

km and to a lesser extent the density between 100 and 400 km. By ${}_0S_{20}$ (Figure 26) the maximum in the shear velocity perturbation has moved up to the region between 400 and 1100 km and the density maximum to 50 and 200 km. The properties of the mantle below about 1000 km has little effect on these modes. Mode ${}_0S_{35}$ is only influenced by

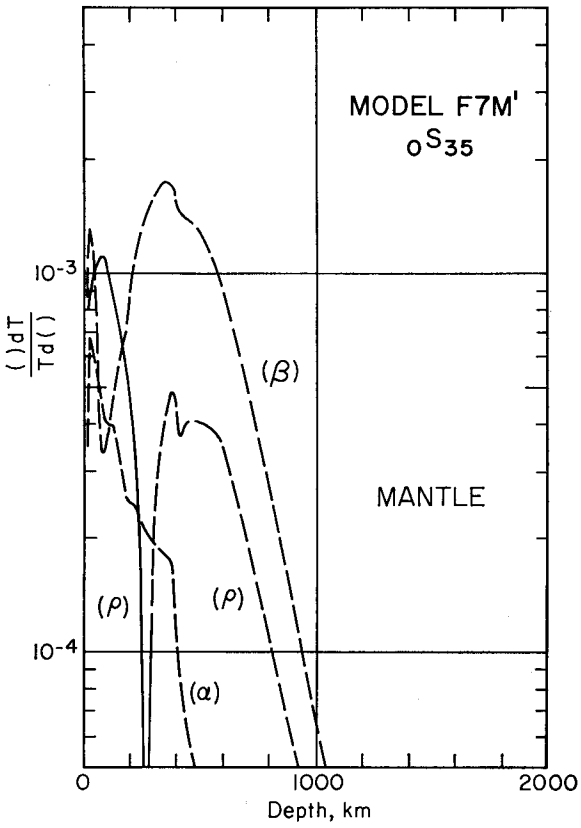

FIG. 27. Variational parameters for ${}_0S_{35}$ as a function of depth.

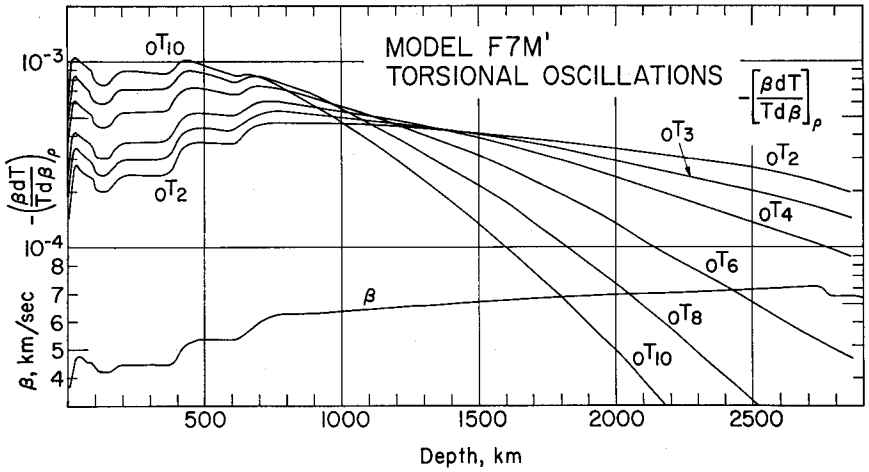

FIG. 28. Shear velocity variational parameters as a function of depth for modes ${}_0T_2$ through ${}_0T_{10}$ as a function of depth. The lower curve is the shear velocity as a function of depth. The fine structure of the normalized variational parameter curves reflects the structure of the model.

properties in the upper 800 km of the earth (Figure 27). Density is important between 50 and 200 km.

The behavior of the partial derivatives for the torsional modes of oscillation are shown in Figures 28 through 30. Modes ${}_0T_2$ through ${}_0T_{10}$ sample the shear velocity rela-

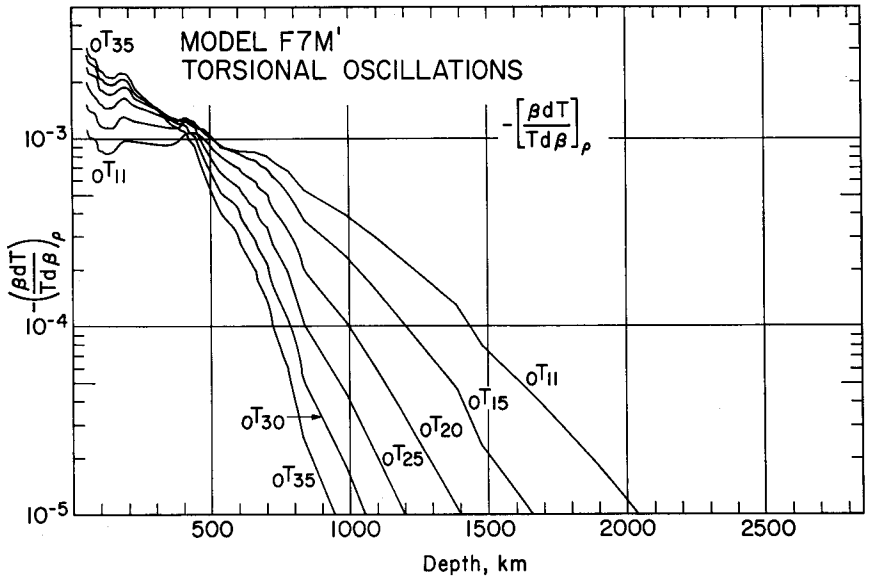

FIG. 29. Shear velocity variational parameters as a function of depth for modes ${}_0T_{11}$ through ${}_0T_{30}$.

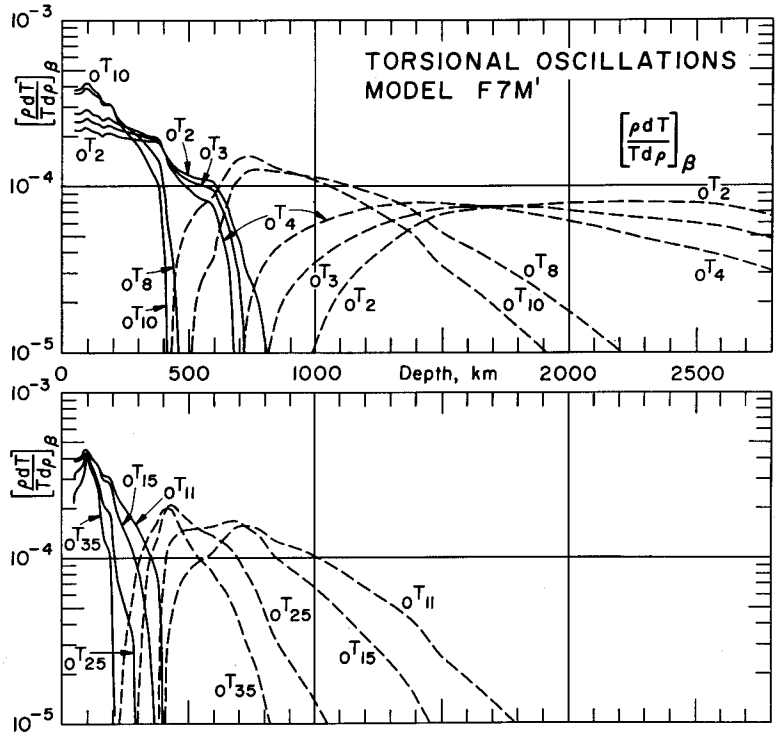

FIG. 30. Density variational parameters as a function of depth for modes ${}_0T_2$ through ${}_0T_{10}$ (upper plot) and ${}_0T_{11}$ through ${}_0T_{35}$ (lower plot). Negative values are shown as dashed lines.

TABLE 3

$(\beta\, dT/T\, d\beta)_{\alpha,\rho}$ Model F7M′ Spheroidal Modes

	Depth (km)	${}_0S_0$	${}_0S_2$	${}_0S_3$	${}_0S_4$	${}_0S_5$	${}_0S_6$	${}_0S_7$	${}_0S_8$	${}_0S_9$	S_{10}	${}_0S_{11}$	${}_0S_{12}$	${}_0S_{13}$	${}_0S_{20}$	${}_0S_{35}$
1	0–7	−.00008	−.00022	−.00046	−.00061	−.00072	−.00084	−.00101	−.00125	−.00153	−.00178	−.00199	−.00218	−.00235	−.00340	−.00617
2	7–56.5	−.00106	−.00309	−.00617	−.00813	−.00938	−.01077	−.01280	−.01557	−.01862	−.02132	−.02347	−.02518	−.02659	−.03337	−.04680
3	56.5–150	−.00104	−.00464	−.00873	−.01104	−.01220	−.01334	−.01499	−.01715	−.01927	−.02077	−.02156	−.02184	−.02177	−.01908	−.04120
4	150–190	−.00030	−.00198	−.00354	−.00430	−.00456	−.00474	−.00500	−.00530	−.00549	−.00545	−.00522	−.00488	−.00451	−.00402	−.02952
5	190–375	−.00052	−.01067	−.01735	−.01971	−.01938	−.01832	−.01712	−.01572	−.01404	−.01248	−.01157	−.01161	−.01277	−.05946	−.27617
6	375–415	+.00004	−.00262	−.00389	−.00420	−.00386	−.00330	−.00267	−.00202	−.00149	−.00130	−.00157	−.00232	−.00351	−.02239	−.06145
7	415–610	+.00152	−.01418	−.01892	−.01958	−.01714	−.01377	−.01055	−.00852	−.00915	−.01341	−.02110	−.03162	−.04443	−.16129	−.22868
8	610–670	+.00065	−.00507	−.00613	−.00603	−.00510	−.00403	−.00330	−.00345	−.00503	−.00810	−.01227	−.01713	−.02238	−.05428	−.03915
9	670–775	+.00162	−.00976	−.01080	−.01048	−.00891	−.00735	−.00685	−.00860	−.01351	−.02112	−.03023	−.03990	−.04954	−.09213	−.04316
10	775–1475	+.02785	−.08505	−.09234	−.10649	−.11794	−.13306	−.16117	−.20910	−.27121	−.33010	−.37400	−.40147	−.41476	−.29678	−.04065
11	1475–2650	+.08851	−.28571	−.32634	−.38255	−.42720	−.45187	−.45067	−.41870	−.36108	−.29500	−.23440	−.18351	−.14208	−.01727	−.00006
12	2650–2750	+.00826	−.03711	−.03994	−.03644	−.03144	−.02668	−.02180	−.01621	−.01042	−.00585	−.00302	−.00149	−.00073	0	0
13	2750–2825	+.00615	−.02761	−.03141	−.02908	−.02458	−.01983	−.01511	−.01039	−.00620	−.00326	−.00159	−.00075	−.00034	0	0
14	2825–2888	+.00515	−.03256	−.04360	−.04503	−.04204	−.03697	−.02992	−.02106	−.01234	−.00617	−.00281	−.00122	−.00053	0	0

TABLE 4

$(\alpha\, dT/T\, d\alpha)_{\beta,\rho}$ Model F7M′ Spheroidal Modes

	Depth (km)	${}_0S_0$	${}_0S_2$	${}_0S_3$	${}_0S_4$	${}_0S_5$	${}_0S_6$	${}_0S_7$	${}_0S_8$	${}_0S_9$	${}_0S_{10}$	${}_0S_{11}$	${}_0S_{12}$	${}_0S_{13}$	${}_0S_{20}$	${}_0S_{35}$
1	0–7	−.00007	−.00019	−.00032	−.00004	−.00038	−.00041	−.00048	−.00058	−.00070	−.00080	−.00089	−.00096	−.00103	−.00146	−.00257
2	7–56.5	−.00119	−.00270	−.00459	−.00515	−.00544	−.00597	−.00695	−.00841	−.01006	−.01155	−.01275	−.01374	−.01461	−.01962	−.02959
3	56.5–150	−.00268	−.00433	−.00731	−.00823	−.00879	−.00978	−.01155	−.01413	−.01704	−.01963	−.02169	−.02333	−.02473	−.03144	−.03626
4	150–190	−.00138	−.00182	−.00304	−.00342	−.00366	−.00408	−.00483	−.00592	−.00713	−.00818	−.00899	−.00960	−.01009	−.01189	−.01073
5	190–375	−.01008	−.00963	−.01588	−.01784	−.01919	−.02155	−.02564	−.03149	−.03790	−.04330	−.04724	−.05006	−.05214	−.05617	−.03709
6	375–415	−.00306	−.00257	−.00414	−.00456	−.00481	−.00530	−.00616	−.00737	−.00865	−.00963	−.01026	−.01062	−.01081	−.00993	−.00475
7	415–610	−.01964	−.01415	−.02219	−.02389	−.02466	−.02649	−.02999	−.03485	−.03959	−.04271	−.04404	−.04416	−.04353	−.03141	−.00845
8	610–670	−.00746	−.00457	−.00695	−.00728	−.00733	−.00767	−.00842	−.00947	−.01040	−.01084	−.01083	−.01052	−.01007	−.00594	−.00103
9	670–775	−.01526	−.00880	−.01301	−.01326	−.01295	−.01308	−.01381	−.01488	−.01563	−.01562	−.01497	−.01398	−.01287	−.00582	−.00061
10	775–1475	−.14676	−.04281	−.05598	−.05251	−.04829	−.04629	−.04623	−.04662	−.04532	−.04158	−.03646	−.03116	−.02626	−.00677	−.00027
11	1475–2650	−.36502	−.01656	−.01495	−.01471	−.01493	−.01415	−.01226	−.00962	−.00691	−.00473	−.00319	−.00214	−.00143	−.00007	0
12	2650–2750	−.03279	−.00012	−.00226	−.00497	−.00652	−.00681	−.00596	−.00426	−.00243	−.00114	−.00048	−.00019	−.00008	0	0
13	2750–2825	−.02480	−.00022	−.00250	−.00525	−.00698	−.00751	−.00682	−.00508	−.00302	−.00149	−.00066	−.00027	−.00011	0	0
14	2825–2888	−.02076	−.00026	−.00233	−.00483	−.00654	−.00723	−.00676	−.00518	−.00317	−.00161	−.00073	−.00031	−.00013	0	0
15	2888–3977	−.35426	−.00002	−.00041	−.00227	−.00448	−.00585	−.00576	−.00428	−.00238	−.00105	−.00041	−.00015	−.00007	0	0
16	3977–4777	−.18064	−.00004	0	0	0	0	0	0	0	0	0	0	0	0	0
17	4777–5025	−.03573	−.00001	0	0	0	0	0	0	0	0	0	0	0	0	0
18	5025–6371	−.05075	−.00132	0	0	0	0	0	0	0	0	0	0	0	0	0

TABLE 5

$(\rho\, dT/T\, d\rho)_{\alpha,\beta}$ Model F7M′ Spheroidal Modes

	Depth (km)	${}_0S_0$	${}_0S_2$	${}_0S_3$	${}_0S_4$	${}_0S_5$	${}_0S_6$	${}_0S_7$	${}_0S_8$	${}_0S_9$	${}_0S_{10}$	${}_0S_{11}$	${}_0S_{12}$	${}_0S_{13}$	${}_0S_{20}$	${}_0S_{35}$
1	0–7	+.00133	+.00075	+.00074	+.00074	+.00081	+.00096	+.00122	+.00160	+.00201	+.00237	+.00266	+.00290	+.00312	+.00468	+.00724
2	7–56.5	+.01045	+.00476	+.00353	+.00297	+.00320	+.00404	+.00550	+.00759	+.00991	+.01196	+.01359	+.01500	+.01634	+.02737	+.04740
3	56.5–150	+.01878	+.00908	+.00767	+.00712	+.00780	+.00959	+.01264	+.01699	+.02189	+.02629	+.02990	+.03303	+.03600	+.05803	+.08728
4	150–190	+.00795	+.00382	+.00327	+.00308	+.00339	+.00417	+.00549	+.00736	+.00947	+.01137	+.01291	+.01423	+.01545	+.02298	+.02371
5	190–375	+.03790	+.01763	+.01492	+.01415	+.01581	+.01957	+.02571	+.03414	+.04327	+.05090	+.05643	+.06039	+.06330	+.06326	−.01580
6	375–415	+.00853	+.00376	+.00311	+.00299	+.00342	+.00432	+.00570	+.00753	+.00939	+.01079	+.01161	+.01197	+.01198	+.00545	−.01623
7	415–610	+.03881	+.01570	+.01242	+.01200	+.01426	+.01844	+.02438	+.03148	+.03769	+.04091	+.04946	+.03859	+.03447	−.01778	−.07546
8	610–670	+.01144	+.00435	+.00351	+.00356	+.00433	+.00557	+.00715	+.00875	+.00972	+.00955	+.00836	+.00649	+.00419	−.01346	−.01515
9	670–775	+.01853	+.00625	+.00495	+.00524	+.00671	+.00880	+.01119	+.01321	+.01375	+.01223	+.00909	+.00503	+.00051	−.02606	−.01714
10	775–1475	+.08085	+.02434	+.02196	+.01845	+.01643	+.01354	+.00580	−.01101	−.03698	−.06555	−.09023	−.10882	−.12150	−.10892	−.01699
11	1475–2650	−.01612	−.05925	−.06224	−.07848	−.09688	−.11304	−.12462	−.12858	−.12249	−.10824	−.09072	−.07349	−.05817	−.00751	−.00002
12	2650–2750	−.00752	−.01463	−.01606	−.01423	−.01162	−.00930	−.00735	−.00548	−.00365	−.00215	−.00116	−.00059	−.00030	0	0
13	2750–2825	−.00594	−.01141	−.01376	−.01287	−.01075	−.00851	−.00639	−.00440	−.00267	−.00144	−.00072	−.00034	−.00016	0	0
14	2825–2888	−.00523	−.01481	−.02070	−.02156	−.02013	−.01770	−.01436	−.01019	−.00605	−.00307	−.00142	−.00062	−.00028	0	0
15	2888–3977	−.08203	+.00620	+.02879	+.04893	+.05648	+.05420	+.04431	+.02964	+.01572	+.00690	+.00273	+.00103	+.00046	0	0
16	3977–4777	−.07309	+.00011	+.00201	+.00189	+.00112	+.00054	+.00022	+.00007	+.00002	0	0	0	0	0	0
17	4777–5025	−.01639	0	0	0	0	0	0	0	0	0	0	0	0	0	0
18	5025–6371	−.02420	−.00068	0	0	0	0	0	0	0	0	0	0	0	0	0

TABLE 6

$\beta\, dT/T\, d\beta$ Model F7M′ Toroidal Modes

	Depth (km)	${}_0T_2$	${}_0T_3$	${}_0T_4$	${}_0T_5$	${}_0T_6$	${}_0T_7$	${}_0T_8$	${}_0T_9$	${}_0T_{10}$	${}_0T_{11}$	${}_0T_{12}$	${}_0T_{13}$	${}_0T_{14}$
1	0–7	−.00103	−.00125	−.00154	−.00187	−.00224	−.00263	−.00303	−.00344	−.00386	−.00427	−.00469	−.00510	−.00551
2	7–56.5	−.01380	−.01678	−.02063	−.02514	−.03008	−.03529	−.04068	−.04617	−.05172	−.05730	−.06286	−.06838	−.07383
3	56.5–150	−.02050	−.02500	−.03081	−.03759	−.04500	−.05276	−.06076	−.06887	−.07703	−.08518	−.09325	−.10121	−.10903
4	150–190	−.00893	−.01091	−.01382	−.01643	−.01965	−.02300	−.02640	−.02981	−.03321	−.03657	−.03986	−.04306	−.04615
5	190–415	−.05707	−.06997	−.08629	−.10479	−.12429	−.14392	−.16319	−.18178	−.19953	−.21629	−.23199	−.24655	−.25997
6	415–610	−.07105	−.08478	−.10123	−.11860	−.13537	−.15064	−.16396	−.17521	−.18441	−.19162	−.19697	−.20064	−.20278
7	610–670	−.02397	−.02809	−.03282	−.03752	−.04169	−.04510	−.04767	−.04942	−.05043	−.05077	−.05055	−.04984	−.04875
8	670–775	−.04875	−.05587	−.06367	−.07095	−.07688	−.08109	−.08361	−.08458	−.08413	−.08274	−.08040	−.07740	−.07391
9	775–1475	−.31192	−.33419	−.35163	−.35906	−.35522	−.34174	−.32136	−.29677	−.27014	−.24310	−.21617	−.19191	−.16892
10	1475–2650	−.38961	−.33519	−.27383	−.21418	−.16220	−.12008	−.08750	−.06303	−.04500	−.03191	−.02250	−.01579	−.01104
11	2650–2750	−.02399	−.01718	−.01098	−.00637	−.00343	−.00175	−.00086	−.00041	−.00019	−.00009	−.00004	−.00002	−.00001
12	2750–2825	−.01639	−.01161	−.00731	−.00416	−.00219	−.00108	−.00051	−.00024	−.00011	−.00005	−.00002	−.00001	0
13	2825–2888	−.01288	−.00908	−.00569	−.00321	−.00167	−.00082	−.00038	−.00017	−.00008	−.00003	−.00001	−.00001	0

TABLE 7

$\rho\, dT/T\, d\rho$ MODEL F7M′ TORSIONAL MODES

	Depth (km)	${}_0T_2$	${}_0T_3$	${}_0T_4$	T_5	${}_0T_6$	${}_0T_7$	${}_0T_8$	${}_0T_9$	${}_0T_{10}$	${}_0T_{11}$	${}_0T_{12}$	${}_0T_{13}$	${}_0T_{14}$
1	0–7	+.00166	+.00190	+.00218	+.00245	+.00272	+.00296	+.00318	+.00338	+.00356	+.00372	+.00387	+.00400	+.00412
2	7–56.5	+.01076	+.01212	+.01359	+.01496	+.01612	+.01704	+.01775	+.01826	+.01861	+.01882	+.01900	+.01886	+.01873
3	56.5–150	+.02018	+.02277	+.02558	+.02826	+.03059	+.03254	+.03412	+.03538	+.03638	+.03713	+.03768	+.03804	+.03824
4	150–190	+.00811	+.00904	+.01001	+.01089	+.01160	+.01213	+.01250	+.01274	+.01287	+.01291	+.01287	+.01277	+.01260
5	190–415	+.04294	+.04604	+.04868	+.05021	+.05049	+.04965	+.04795	+.04562	+.04283	+.03973	+.03646	+.03310	+.02972
6	415–610	+.02355	+.02232	+.01982	+.01606	+.01138	+.00619	+.00086	−.00434	−.00926	−.01378	−.01785	−.02143	−.02453
7	610–670	+.00533	+.00447	+.00318	+.00156	−.00022	−.00198	−.00364	−.00511	−.00637	−.00742	−.00824	−.00864	−.00930
8	670–775	+.00457	+.00257	−.00014	−.00319	−.00630	−.00916	−.01162	−.01361	−.01512	−.01619	−.01686	−.01718	−.01720
9	775–1475	−.01302	−.02718	−.04218	−.05519	−.06450	−.06979	−.07154	−.07057	−.06767	−.06353	−.05866	−.05349	−.04828
10	1475–2650	−.08731	−.08179	−.07273	−.06126	−.04927	−.03822	−.02888	−.02140	−.01562	−.01128	−.00808	−.00574	−.00406
11	2650–2750	−.00751	−.00553	−.00365	−.00219	−.00121	−.00064	−.00032	−.00015	−.00007	−.00003	−.00002	−.00001	0
12	2750–2825	−.00514	−.00374	−.00243	−.00142	−.00077	−.00039	−.00019	−.00009	−.00004	−.00002	−.00001	0	0
13	2825–2888	−.00406	−.00294	−.00189	−.00110	−.00059	−.00029	−.00014	−.00006	−.00003	−.00001	0	0	0

tively uniformly in the upper 1000 km of the earth. ${}_0T_2$ samples the shear velocity of the whole mantle almost uniformly. The shear velocity perturbation parameter is concentrated more and more towards the surface as the mode number increases; for example, ${}_0T_{35}$ only effectively samples the shear velocity distribution above 500 km. The very low-order torsional oscillations are also effected, to a lesser extent, by the density distribution in the upper 500 km, and change sign in the upper mantle.

Partial Derivative Tables

The main purpose of this paper is to indicate in a qualitative manner which parameters of the Earth are contributing to the various modes of free oscillation. The figures

TABLE 8

Interval Mass and Moment of Inertia

	Depth (km)	Mass (10^{28} gm)	Moment (10^{36} gm kg m)
1	0–7	.00101	.00273
2	7–56.5	.00830	.02224
3	56.5–150	.01464	.03835
4	150–190	.00620	.01588
5	190–375	.03023	.07472
6	375–415	.00702	.01671
7	415–610	.03386	.07750
8	610–670	.01057	.02315
9	670–775	.01838	.03909
10	775–1475	.11050	.20383
11	1475–2650	.13976	.17741
12	2650–2750	.00912	.00820
13	2750–2825	.00656	.00562
14	2825–2888	.00532	.00438
15	2888–3977	.12691	.07651
16	3977–4777	.04809	.01353
17	4777–5025	.00826	.00121
18	5025–6371	.01290	.00093
Total		0.59763×10^{28}	0.80199×10^{36}

in the previous section allow one to determine the sensitivity of a given mode to the parameters in the various regions of the Earth and, in a crude way, to access the resolving power of the various modes.

The partial derivatives also permit one to modify the standard model in such a way as to force agreement, to first order, between the computed and observed free oscillation spectrum. Since the modes discussed in this paper have relatively low resolving power we tabulate the partial derivatives, or variational parameters, for the 18 major regions of the standard model which were discussed previously. The partial derivatives, integrated over the region noted, are tabulated in Tables 3 through 8. The regions correspond to (1) the crust; (2) the lid of the low-velocity zone; (3) the low-velocity zone; (4) and (5), the region between the low-velocity zone and the top of the C-region; (6) the first major upper mantle transition region; (7) the homogeneous region between the upper mantle discontinuities; (8) the second major transition region of the mantle; (9) the region below this transition to allow for a possible discontinuity near 800 km; (10) the upper part of the lower mantle; (11) the lower part of that part of the lower mantle which seems to be relatively homogeneous; (12), (13) and (14) have been

treated separately to allow for inhomogeneity near the base of the mantle and to allow for a possible increase in core radius; (15) the outer part of the outer core; (16) the inner part of the outer core where some heterogeneity may be involved; (17) the transition region between the inner and outer cores; and (18) the entire inner core.

Each of these regions may be perturbed as a whole simply by multiplying the entry in the table by the fractional change in the parameter. For example, a 10% increase in the shear velocity of the low-velocity zone (Row 3 in Tables 3 through 7) will decrease the periods of ${}_0S_0$, ${}_0S_2$, ${}_0S_3$, ${}_0S_{20}$ by 0.010%, 0.046%, 0.087% and 0.191% respectively (see Table 3). The inverse problem has been discussed in previous papers of this series.

Table 8 gives the mass and moment of inertia of these 18 regions. This table is required when density perturbations are made in order to balance the mass and moment of inertia of the Earth.

Conclusions

The variational parameters presented herein for a realistic Earth model enable one to determine at a glance which elastic parameters control a particular period of free oscillation. Several interesting conclusions emerge as a result of this study. The low order fundamental spheroidal modes are particularly sensitive to the shear velocity distribution in the lower mantle; they are not particularly sensitive to the properties of the core. In fact, fundamental mode free oscillation data do not, by themselves, provide compelling constraints for a given density distribution in the lower mantle or core unless these regions are homogeneous and can be treated as units. Everything else being equal a 0.1% error in ${}_0S_0$ leads to an uncertainty of 4 per cent in the density of the inner core and this is not improved by using other fundamental mode data. However, the mode ${}_1S_0$ should prove valuable for delineating density bounds for the inner core. The low order fundamental modes are about as sensitive to the shear velocity in the inner core as they are to the density in this region.

If the distribution of shear velocity in the lower mantle and the compressional velocity in the upper mantle are independently and accurately known the gravest spheroidal modes can be used as constraints on the density distribution in the upper mantle. When torsional oscillation data, which are primarily affected by the shear velocity structure, are combined with spheroidal data additional constraints are provided on the density in the upper mantle.

By comparing the variational parameters as a function of depth for nearby modes it is possible to estimate the degree of independence of these modes. For example, ${}_0S_8$, ${}_0S_9$ and ${}_0S_{10}$ sample the Earth in nearly the same way and these modes do not supply data that, for practical purposes, is independent. The linear independence of a set of free oscillation modes should be tested prior to the inversion of the corresponding data to obtain an Earth model. Clearly, the larger the separation in n the more independent the data. This feature of free oscillation data makes it preferable to use only superior and uncontaminated data in an inversion scheme rather than using all available data.

Acknowledgments

This research was supported by the Advanced Research Projects Agency and was monitored by the Air Force Office of Scientific Research under contracts AF 49(638)-1337 (CIT) and AF 49(638)-1687 (SU). Support was also provided by NASA grant NGL 05-020-232 to Stanford University. The authors wish to acknowledge the assistance of Martin Smith, Tom Jordan, Laszlo Lenches and Shirley Fisher in the preparation of the manuscript.

References

Adams, R. D., and M. J. Randall (1964). The fine structure of the Earth's core, *Bull. Seism. Soc. Am.* **54**, 1299–1313.

Anderson, Don L. (1964). Universal dispersion tables, 1, Love waves across oceans and continents on a spherical Earth, *Bull. Seism. Soc. Am.* **54**, 681–726.

Anderson, Don L., and David G. Harkrider (1968). Universal dispersion tables, 2, Variational parameters for amplitudes, phase velocity and group velocity for first four Love modes for an oceanic and a continental Earth model, *Bull. Seism. Soc. Am.* **58**, 1407–1499.

Anderson, Don L., and M. N. Toksoz (1963). Surface waves on a spherical Earth, 1, Upper mantle structure from Love waves, *J. Geophys. Res.* **68**, 3482–3500.

Archambeau, C. B., and Don L. Anderson (1964). Inversion of surface wave dispersion data, *Serie A, Travaux Scientifiques, FASC.* **23**, 45–54, Publ. du Bureau Central Seismologique International.

Backus, G., and F. Gilbert (1967). Numerical applications of a formalism for geophysical inverse problems, *Geophys. J.* **13**, 247–276.

Gutenberg, B., The boundary of the Earth's inner core (1957). *Trans. Amer. Geophys. Union* **38**, 750–753.

Jeffreys, H. (1935). The surface waves of earthquakes, *Mon. Not. Roy. Astron. Soc. Geophys. Suppl.* **3**, 253–261.

Jeffreys, H. (1939). The times of the core waves, *Mon. Not. Roy. Astron. Soc. Geophys. Suppl.* **4**, 594–615.

Johnson, L. (1967). Array measurements of P velocities in the upper mantle, *J. Geophys. Res.* **72**, 6309–6326.

Stoneley, R. (1926). The elastic yielding of the Earth, *Mon. Not. Roy. Astron. Soc. Geophys. Suppl.* **1**, 356–359.

Takeuchi, H., J. Dorman, and M. Saito (1964). Partial derivatives of surface wave phase velocity with respect to physical parameter changes within the earth, *J. Geophys. Res.* **69**, 3429–3441.

Wiggins, R. A. (1968). Terrestrial variational tables for the periods and attenuation of the free oscillations, *Physics of the Earth and Planetary Interiors* **1**, 20–266.

Seismological Laboratory
California Institute of Technology
Pasadena, California 91109
Division of Geological Sciences
Contribution No. 1613

Department of Geophysics
Stanford University
Stanford, California

Manuscript received February 13, 1969.